Coordinated perimeter flow and variable speed limit control for mixed freeway and urban networks

By

Rebeka Yocum
Department of Civil and Environmental Engineering
The Pennsylvania State University
201 Transportation Research Building
University Park, PA 16802
Phone: 814-863-1897
rly16@psu.edu

Vikash V. Gayah*
Department of Civil and Environmental Engineering
The Pennsylvania State University
231L Sackett Building
University Park, PA 16802
Phone: 814-865-4014
gayah@engr.psu.edu

***Corresponding Author**

July 2021

Word Count: 6,910 (6,410 words + 2 tables)

ABSTRACT

Recent studies have leveraged the existence of network Macroscopic Fundamental Diagrams to develop regional control strategies for urban traffic networks. Existing MFD-based control strategies focus on vehicle movement within and across regions of an urban network and do not consider how freeway traffic can be controlled to improve overall traffic operations in mixed freeway and urban networks. The purpose of this study is to develop a coordinated traffic management scheme that simultaneously implements perimeter flow control on an urban network and variable speed limits on a freeway to reduce total travel time in such a mixed network. By slowing down vehicles traveling along the freeway, variable speed limits can effectively meter traffic exiting the freeway into the urban network. This can be particularly useful since freeways often have large storage capacities and vehicles accumulating on freeways might be less disruptive to overall system operations than doing so on urban streets. Variable speed limits can also be used to change where freeway vehicles enter the urban network to benefit the entire system. The combined control strategy is implemented in a model predictive control framework with several realistic constraints, such as gradual reductions in freeway speed limit. Numerical tests suggest that the combined implementation of variable speed limits and perimeter metering control can improve traffic operations compared to perimeter metering alone.

INTRODUCTION

Management of freeway and surface streets is a topic of great interest to the traffic flow community. A variety of strategies have been proposed and tested to improve traffic performance on freeways, including on-ramp metering (*1–3*) and variable speed limits (*4–6*), among others. These congestion management strategies are often applied to mitigate congestion on individual freeway bottlenecks. On the urban street side, control strategies generally focus on adjusting signal timings at individual intersections (*7–10*) , since signals serve as the most common bottlenecks on urban streets. Isolated urban networks and freeways are not representative of the mixed networks that exist in which freeways and urban networks interact. While it is beneficial to consider congestion management strategies that control vehicles across these different roadway types, coordinating traffic management across freeways and urban streets has generally been difficult due to the complexity of describing traffic across these different roadway types using traditional methods.

Recent advances in modeling large-scale urban traffic networks may serve as a bridge to coordinate traffic control across freeways and urban networks as they provide a more computationally efficient way to describe traffic behavior from a regional perspective. These methods rely on the existence of well-defined relationships between traffic variables across spatially compact regions (*11–13*)—known more commonly as network Macroscopic Fundamental Diagrams (NFDs or MFDs)—that arise under certain conditions (*14*, *15*). Leveraging knowledge of these MFDs to model urban traffic network dynamics (*16*) allows for the development of elegant network-wide congestion management strategies in which entire networks can be managed without controlling individual intersections within the region. Previous studies have implemented MFD-based frameworks to develop various regional-level urban traffic control strategies. Examples of these strategies include perimeter flow control/metering (*17–23*), pricing (*24–27*), and street network design (*28–31*), among others (*32*, *33*).

To the authors' knowledge, only one study used an MFD-based framework to develop a coordinated traffic management scheme for freeways and urban networks (*34*). Perimeter flow control and on-ramp metering were simultaneously implemented to improve the combined total travel time experienced on both. The proposed strategy determined optimal rates vehicles were allowed to travel between regions of an urban network (perimeter flow control/metering), as well as rates vehicles were allowed to move between the urban network and freeway (via on-ramp metering). The combination of this joint freeway/urban network control was found to improve traffic conditions on the combined network. However, this strategy only limited vehicle movement between the urban regions and from the urban region to the freeway; it did not consider limiting vehicle movement from the freeway to the urban network. Thus, an important piece is missing from the previous work surrounding congestion management in mixed networks: managing the vehicles exiting the freeway and entering the urban region.

The purpose of this study is to develop a coordinated traffic management scheme that simultaneously implements perimeter flow control on the urban network and variable speed limits on the freeway. As will be shown, variable speed limits can limit how vehicles are able to move from the freeway to the urban network, which serves as a surrogate form of metering. While a similar effect can be achieved by metering the rate vehicles can exit the freeway (either at the ramp location or downstream where the ramp connects with the surface streets), VSL control does not require vehicles from the freeway to completely stop, which could lead to long queues and unnecessary congestion or queue spillover to freeway itself. Instead, it simply changes the speed

and density at which vehicles travel along the freeway. This might be useful in specific situations since freeways often have large storage capacities and vehicles accumulating on freeways might be less disruptive than vehicles accumulating on urban streets. VSL can also make it less attractive to enter the urban network from some locations as opposed to others, which can be leveraged to produce further travel time savings. Note, however, that VSL control only impacts vehicles traveling on the freeway, while perimeter metering control only impacts demand traveling between two urban regions. The combination of control strategies does not impact demand traveling within each urban region. The proposed VSL-perimeter metering control scheme is integrated into an MPC optimization framework for networks governed by MFDs. The framework is used to compare the effectiveness of VSL control, perimeter metering control, and a combination of the two as a means to manage congestion in a mixed network made up of urban regions and a freeway.

The remainder of this paper is organized as follows: first, the methodology is outlined; then, three numerical examples are presented; finally, a discussion of the results and future work is provided.

METHODOLOGY

In this work, we consider a system that consists of a freeway and an urban network, the latter of which can be partitioned into two homogenous urban regions. Such partitioning has been shown to produce more reliable and well-defined MFDs (*35*). A schematic representation of the system considered here is shown in Figure 1. It is assumed that different off-ramps exist through which vehicles can exit the freeway and travel into region 1 and region 2. Note that this configuration is selected to demonstrate the benefits of the proposed VSL and gating strategy when route choice is present; however, the overall methodology is general and can be applied to other system configurations.

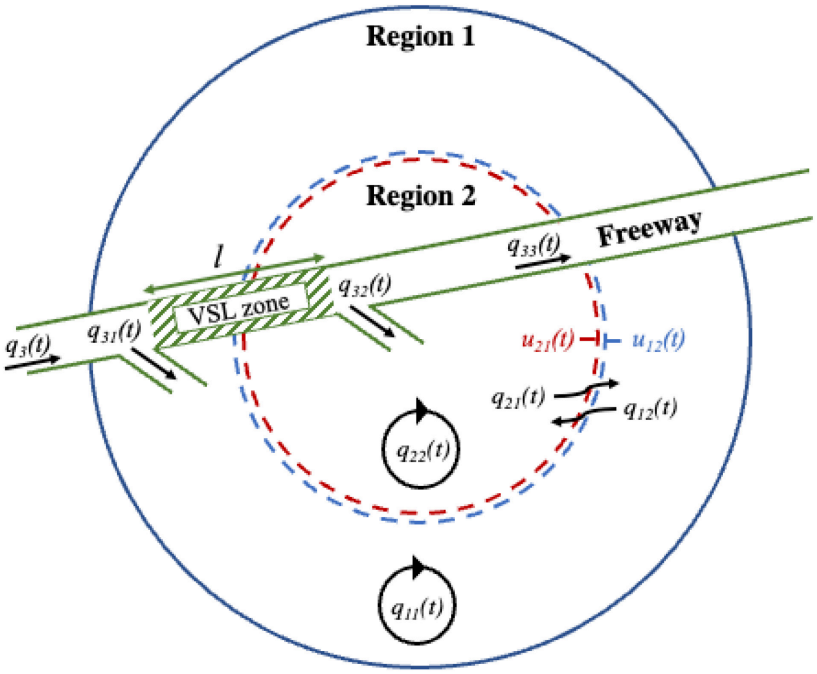

Figure 1. Schematic representation of an example two urban region and freeway network

Traffic within the two urban regions ($i = 1$ for region 1, $i = 2$ for region 2) is assumed to be described by well-defined MFDs that relate accumulation in region i, $n_i(t)$, with the trip completion rate in that region, $G_i(n_i(t))$. Vehicle movement between the two urban regions is managed using perimeter metering control. The controllers, expressed as $u_{12}(t)$ and $u_{21}(t)$, limit the proportion of vehicles wishing to move between the two regions that are actually able to do so. For example, a control value of $u_{12}(t) = 0.6$ means that 60% of vehicles that wish to move from region 1 to region 2 are permitted to do so while the other 40% are held back and can only transfer between the two regions at a later time. Traffic on the freeway ($i = 3$) is managed using variable speed limits (VSL) where a speed limit is implemented within a designated zone (shown in Figure 1) at each time step, t. The effect of the implementation of VSL on freeway traffic will be described in a later section.

Regions 1 and 2 experience endogenous demands expressed as $q_{11}(t)$ and $q_{22}(t)$, respectively, and exogenous demands expressed as $q_{12}(t)$ and $q_{21}(t)$, respectively. We assume that the freeway operates in free flow and no active bottlenecks exist. The total freeway demand is expressed as $q_3(t)$, with some portion of vehicles exiting the freeway into the urban network and the remaining vehicles continuing on. Freeway vehicles that enter the urban network are either destined for region 1 or region 2, and the corresponding demands are expressed as $q_{31}(t)$ and $q_{32}(t)$, respectively. The demand that does not exit the freeway is expressed as $q_{33}(t)$ where:

$$q_3(t) = q_{31}(t) + q_{32}(t) + q_{33}(t). \quad (1)$$

Implementation of route choice

A tabular summary of the possible routes for vehicles traveling through the mixed network shown in Figure 1 is provided in Table 1. Note that vehicles exiting the freeway into regions 1 and 2 have a choice in potential routes to take. Thus, it is critical to account for vehicle routing behavior. The network structure shown in Figure 1 lends itself to a simplistic route choice formulation, where vehicles only have two route options when traveling through different parts of the network. Here, we assume that travelers select a route that minimizes their own personal travel time.

Table 1. Tabular representation of route choice in the mixed network

Origin	Destination		
	Region 1 ($i = 1$)	**Region 2 ($i = 2$)**	**Freeway ($i = 3$)**
Region 1	$1 \rightarrow 1$	$1 \rightarrow 2$	N/A
Region 2	$2 \rightarrow 1$	$2 \rightarrow 2$	N/A
Freeway	$3 \rightarrow 1$, $3 \rightarrow 2 \rightarrow 1$	$3 \rightarrow 2$, $3 \rightarrow 1 \rightarrow 2$	$3 \rightarrow 3$

Let $\theta_1 \in [0,1]$ be the portion of vehicles wishing to exit the freeway into region 1 that exit into region 1 directly. Similarly, let $\theta_2 \in [0,1]$ be the portion of vehicles wishing to exit the freeway into region 2 that exit into region 2 directly. Following these definitions, it is clear that $1-\theta_1$ and $1-\theta_2$ represent the portion of vehicles wishing to exit into regions 1 and 2, respectively, that opt to take the alternate route available to them. It is assumed that travelers choose their route to minimize their own personal travel time, thus, θ_1 and θ_2 are dependent on the travel time throughout the network. The travel time for each route is equivalent to the sum of individual travel times through element i along the route. Total and average travel times in regions 1 and 2 are expressed in (2) and (3), respectively. Travel time from ramp 1 to ramp 2 goes through the VSL zone (length $l\ mi$) and thus is dependent upon the VSL control value; see (4). Using (2-4), $\theta_1(t)$ and $\theta_2(t)$ are estimated using the softmax function (5-6). $\theta_1(t)$ can be considered the probability that travel time along route $3 \rightarrow 1$ is shorter than travel time along route $3 \rightarrow 2 \rightarrow 1$. This same logic applies to $\theta_2(t)$.

$$t_1(t) = \frac{1}{G_1(n_1(t))}, t_2(t) = \frac{1}{G_2(n_2(t))} \quad (2)$$

$$\overline{t_1}(t) = \frac{1}{G_1(n_1(t))}, \overline{t_2}(t) = \frac{1}{G_2(n_2(t))} \quad (3)$$

$$\overline{t_l}(t) = \frac{l}{VSL(t)} \quad (4)$$

$$\theta_1\big(VSL(t), n_1(t), n_2(t)\big) = \frac{e^{-\gamma * \overline{tt}_{31}}}{e^{-\gamma * \overline{tt}_{31}} + e^{-\gamma * \overline{tt}_{321}}} \quad (5)$$

$$\theta_2\big(VSL(t), n_1(t), n_2(t)\big) = \frac{e^{-\gamma * \overline{tt}_{32}}}{e^{-\gamma * \overline{tt}_{32}} + e^{-\gamma * \overline{tt}_{312}}} \quad (6)$$

For the purposes of this work, θ_1 is taken to always be 1. This is due to the geometric aspects of the network (shown in Figure 1), which leads to the travel time from the freeway directly into region 1 generally being much shorter than that from the freeway to region 2 and then into region 1. With $\theta_1 = 1$, all vehicles wishing to exit the freeway into region 1 do so directly.

Implementation of variable speed limits

The effect of variable speed limit control on free flow freeway traffic is predicted using LWR theory (*36–39*). We assume traffic on the freeway can be described using a triangular fundamental diagram (FD), as illustrated in Figure 2a. We also assume the VSL control is implemented within a specific "zone" along the freeway and that speeds are only allowed to change at discrete points in time. These spatial and temporal constraints allow us to estimate the impact of changing the speed limit on freeway traffic graphically using time space diagrams. It is assumed that all vehicles obey the VSL guidance and are aware of speed limit changes as they are made. Such VSL implementation could be achieved using regularly spaced dynamic VSL signs or using Connected Vehicle technology (*6*). The effects of non-compliance could be integrated by modeling only the change in average speed and selecting the corresponding speed limit that would achieve the desired average travel speed. Note that previous research has found small changes in speed limit would generally be accepted by travelers, while larger reductions in speed limit are more likely to be ignored (*40*). Finally, it is assumed that variable speed limits are only implemented when the freeway is operating under freely flowing traffic conditions as reducing the speed limit would be less effective at managing traffic if vehicles are already traveling at congested speeds. However,

it is possible for VSL to be implemented and have an effect by reducing the speed limit even further than the congested travel speeds. The same basic steps and methodology can be applied for this case.

Under these assumptions, changes in speed limit at a point in space are represented by a horizontal interface on the time space diagram, and changes in speed limit at a point in time are represented using a vertical interface on the time space diagram, similar to the work presented in (*36*). Consider a known freeway traffic demand, where vehicles are traveling in free-flow conditions. A lower speed within a specific region of time and space results in traffic states that are associated with a second free flow branch on the FD, as shown in Figure 2b. Thus, lowering the speed limit should generate three interfaces: one horizontal, one vertical, and one traveling at the newly implemented speed limit. These interfaces are illustrated as dark red lines on the time space diagram that accompanies the FD in Figure 2b. The lighter lines represent individual vehicle trajectories and how they would change in response to the changes in the speed limit. Notice that lowering the speed limit causes an initial reduction in flow as vehicles within the lower-speed limit zone reduce their speed but maintain their density. However, the flow of vehicles entering at the reduced-speed limit stays the same as vehicles simply adjust their speed and corresponding travel density upon entering this section.

Similar interfaces arise when the speed limit is increased; see Figure 2c. Traffic states only arise on a new free-flow branch of the FD associated with the increased speed. Note that this is equal to the original free-flow branch if the increased speed is equal to the original free-flow speed, but could also result in a new free flow branch if the increased speed limit is smaller than the free-flow speed. Three interfaces again arise when the speed limit is increased: one horizontal, one vertical, and one traveling at the newly implemented speed limit. An example of this transition is shown in Figure 2c. The figure reveals that when the speed limit is increased, the first few vehicles travel at the same density and a higher speed, resulting in a momentary increase in flow, while the following vehicles maintain their flow while traveling at a lower density.

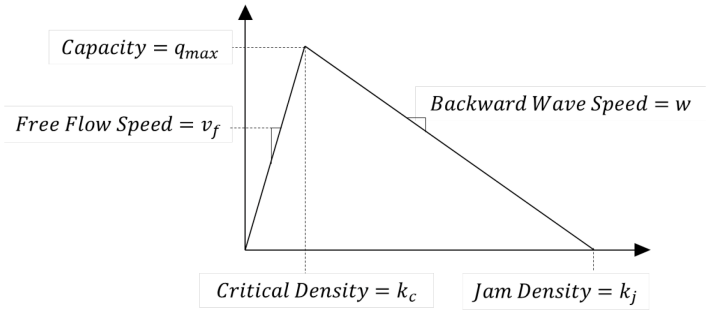

(a) Assumed triangular fundamental diagram

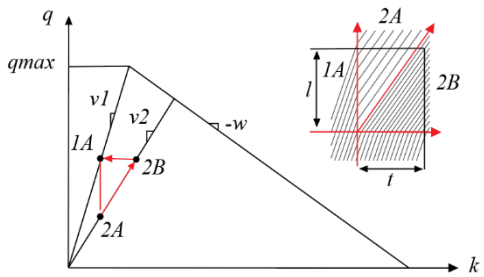

(b) Reduction in speed limit

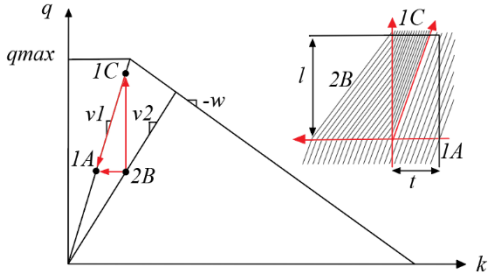

(c) Increase in speed limit

Figure 2. Assumed triangular fundamental diagram and traffic states that arise when speed limit is reduced and increased

A minimum speed limit can be determined to ensure that the freeway flow does not become congested when a lower speed limit is increased. This lower bound ensures that the point 1C in Figure 2c will never lie on the congested branch of the fundamental diagram and is a function of freeway demand, free flow speed, v_f, and the capacity of the freeway, q_{max}:

$$v_{min} = \frac{q_3(t) * v_f}{q_{max}} \tag{7}$$

VSL impacts at second exit ramp

Assuming the exit ramp into region 2 lies at the end of the VSL zone allows us to calculate the average flow passing that exit ramp during any discrete time period as the proportion of time each state occurs on the time space diagram. The length of the VSL zone is determined to ensure that the impact of changing the speed limit during a given time period on traffic flow is fully contained within that time period. This length is:

$$l \leq \frac{q_3(t) * v_f}{q_{max}} t, or\ l \leq v_{min} t \tag{8}$$

Under these conditions, the flow passing the second exit ramp during time period t can be described as a function of the demand entering the VSL zone (q_{zone}), route choice parameters, the speed limit in the previous time period, and the speed limit implemented in time period t:

$$q_{ramp,2}(t) = f(q_{zone}(t), v_{des}(t-1), v_{des}(t)) \tag{9}$$

The flow passing the second exit ramp is calculated using the proportion of time that each traffic state exists at the exit ramp. Considering the speed limit reduction shown in Figure 2b, the flow passing the exit ramp is calculated as shown below.

$$q_{ramp,2} = \left(q_{2A} * \frac{\frac{l}{v_2}}{t}\right) + \left(q_{2B} * \frac{t - \left(\frac{l}{v_2}\right)}{t}\right),$$

where $q_{2A} = k_{2A} * v_2 = \frac{q_{1A}}{v_1} * v_2$ and $q_{2B} = q_{1A}$. Simplification results in the final expression for the ramp passing the exit ramp;

$$q_{ramp,2} = q_{1A}\left(1 + \left(\frac{l}{t*v_1}\right) - \left(\frac{l}{t*v_2}\right)\right).$$

Without loss of generality, consider a case where there are three possible speed limit alternatives (v_1, v_2, v_3), no route choice $(\theta_2(t) = \theta_2(t+1) = 1)$, and a constant freeway demand, where $q_3(t) = q_3(t+1) = q_3 \; \forall \; t$. Under these assumptions, the flow passing the second exit ramp during any time step $t+1$ can be represented in a matrix form as a function of the demand (q_3), speed limits in the current $(v(t))$ and future $(v(t+1))$ time steps and the length of the time interval (Δt); see Table 2. These values are obtained from the geometry of Figure 2b and Figure 2c.

Table 2. Matrix representation of the possible values of freeway flow passing the exit ramp

Speed Limit at Current Time Step (t)	*Speed Limit at Next Time Step (t + 1)*		
	$\mathbf{v_1}$	$\mathbf{v_2}$	$\mathbf{v_3}$
$\mathbf{v_1}$	q_3	$q_3\left[1 + \left(\frac{l}{\Delta t * v_1}\right) - \left(\frac{l}{\Delta t * v_2}\right)\right]$	$q_3\left[1 + \left(\frac{l}{\Delta t * v_1}\right) - \left(\frac{l}{\Delta t * v_3}\right)\right]$
$\mathbf{v_2}$	$q_3\left[1 + \left(\frac{l}{\Delta t * v_2}\right) - \left(\frac{l}{\Delta t * v_1}\right)\right]$	q_3	$q_3\left[1 + \left(\frac{l}{\Delta t * v_2}\right) - \left(\frac{l}{\Delta t * v_3}\right)\right]$
$\mathbf{v_3}$	$q_3\left[1 + \left(\frac{l}{\Delta t * v_3}\right) - \left(\frac{l}{\Delta t * v_1}\right)\right]$	$q_3\left[1 + \left(\frac{l}{\Delta t * v_3}\right) - \left(\frac{l}{\Delta t * v_2}\right)\right]$	q_3

This representation allows for a simple mathematical relationship that can be used to estimate the effect of changing the speed limit on the freeway on traffic flow. The matrix in Table 1 can also be expanded to account for a changing freeway demand and dynamic route choice, as well as more than three possible speed limits. However, differences along the diagonal would have to be incorporated to address the situations where changes passing the exit ramp might occur without an accompanying change in speed limit. The equations in Table 1 can be generalized to account for a changing freeway demand:

$$q_{ramp,2}(t) = q_{zone}(t) + \frac{q_{zone}(t-1)*l}{\Delta t*v(t-1)} - \frac{q_{zone}(t)*l}{\Delta t*v(t)}, \quad (10)$$

where $q_{zone}(t)$ represents the flow entering the VSL zone after vehicles have exited at the first exit ramp. Note may also change $q_{zone}(t)$ due to the implementation of route choice, as seen in (11). The flow $q_{ramp,2}(t)$ is then split according to the destination of the original freeway demands considering route choice (exiting into region 2, continuing on the freeway).

VSL impacts at first exit ramp

Because VSL control is only implemented within the VSL zone outlined previously (between the first and second exit ramps), it is assumed vehicles on the freeway travel at free flow speed before entering the VSL zone. Thus, a change in speed limit within the VSL zone does not impact the flow of vehicles exiting at the first ramp. However, the flow of vehicles exiting at the first ramp does impact the flow of vehicles passing the second exit ramp in the form of q_{zone} introduced previously:

$$q_{zone}(t) = q_3(t) - \left(\theta_1(t) * q_{31}(t)\right) - \left(\left(1 - \theta_2(t)\right) * q_{32}(t)\right) \quad (11)$$

Thus, the VSL control affects the flow of vehicles using exit ramp 2 directly by changing the flow of vehicles in the VSL zone and indirectly by influencing how freeway vehicles destined for region 2 route themselves.

Optimal control problem

The combined VSL and gating control problem becomes a mixed integer nonlinear program (MINLP). The proposed control problem can be solved using an MPC framework as described in (*41*). The MPC framework is a receding horizon framework in which the controller looks far into the future at every time step and determines an optimal set of steps to take; however, only the first set of control actions in the optimal sequence is implemented. Then, the optimization process repeats itself to determine the next set of control actions to implement. The number of time steps that the controller considers in determining the impact of the control during the optimization is the prediction horizon, N_p. Optimal control actions are only obtained for the first subset of these time steps, which is known as the control horizon, N_c. Following (*41*), we use a prediction horizon of twenty time steps and control horizon of two time steps in the MINLP presented in this paper.

Every time the MPC controller solves for an optimal sequence of control actions, it considers the effect of these actions on a given objective function. The objective function considered in this work is the minimization of the total number of vehicles within the network (and thus, minimizes the total travel time) observed during some study period t_0 through t_f. This objective function is mathematically represented by:

$$J = \min_{u_{21}u_{12},v_{des}} \int_{t_0}^{t_f} [\sum n_i(t)]dt, \quad (12)$$

where $\sum n_i(t)$, $i = 1,2,3$ represents the total accumulation in the mixed network during time period t, $n_i(t) = \sum n_{ij}(t)$, $i,j = 1,2$, is the accumulation in region i, $n_3(t) = \sum n_{3k}$, $k = 1,2,3$ is the accumulation on the freeway, and $v_{des} \in \{v_1, v_2, \dots, v_n\}$ is the variable speed limit chosen from

a discrete set of values. Discrete values for the speed limit are chosen to ensure implemented speed limits are not unusual and do not cause confusion to those traveling on the freeway.

Dynamic equations similar to those in (*40*) are used to describe how accumulations within each region change over time. First, it is beneficial to define the parameters below.

$\alpha_1(t) \in (0,1)$	portion of total freeway demand wishing to exit into region 1, at time step t
$\alpha_2(t) \in (0,1)$	portion of freeway demand not exiting at ramp 1 wishing to exit into region 2, at time step t
$\beta(t) \in (0,1)$	portion of freeway demand not exiting at ramp 1 wishing to continue on freeway, at time step t

Equations (13-14) provide the dynamic equations that show how accumulation of vehicles within region 1 destined for region 1, and region 2 changes in time. Equations (15-16) provide the dynamic equations that show how accumulation of vehicles within region 2 destined for region 2 and region 1 changes in time. Equations (17-19) show how the accumulation of vehicles on the freeway destined for region 1, and region 2 changes, as well as how the accumulation of vehicles not wishing to exit the freeway changes.

$$\frac{dn_{11}(t)}{dt} = \left[q_{11}(t) - M11(t) + u_{21}M21(t) + \left(\theta_1(t) * \alpha_1(t) * q_{ramp,1}(t)\right)\right] \quad (13)$$

$$\frac{dn_{12}(t)}{dt} = \left[q_{12}(t) - u_{12}M12(t) + \left(\left(1-\theta_2(t)\right) * \alpha_2(t) * q_{ramp,2}(t)\right)\right] \quad (14)$$

$$\frac{dn_{22}(t)}{dt} = \left[q_{12}(t) - M22(t) + u_{12}M12(t) + \left(\theta_2(t) * \alpha_2(t) * q_{ramp,2}(t)\right)\right] \quad (15)$$

$$\frac{dn_{21}(t)}{dt} = \left[q_{21}(t) - u_{21}M21(t) + \left(\left(1-\theta_1(t)\right) * \alpha_1(t) * q_{ramp,1}(t)\right)\right] \quad (16)$$

$$\frac{dn_{31}(t)}{dt} = \begin{bmatrix} \left(\theta_1(tt) * \left(q_{31}(tt) - \left(\alpha_1(t) * q_{ramp,1}(tt)\right)\right)\right) \\ + \left(\left(1-\theta_2(tt)\right) * \left(q_{32}(tt) - \left(\alpha_2(tt) * q_{ramp,2}(tt)\right)\right)\right) \end{bmatrix} \quad (17)$$

$$\frac{dn_{32}(t)}{dt} = \begin{bmatrix} \left(\theta_2(tt) * \left(q_{32}(tt) - \left(\alpha_2(t) * q_{ramp,2}(tt)\right)\right)\right) + \\ \left(\left(1-\theta_1(tt)\right) * \left(q_{31}(tt) - \left(\alpha_1(tt) * q_{ramp,1}(tt)\right)\right)\right) \end{bmatrix} \quad (18)$$

$$\frac{dn_{33}(t)}{dt} = \left[q_{33}(t) - \beta(t) * q_{ramp,2}(t)\right] \quad (19)$$

The MFD is used to describe how vehicles move between regions in the urban network or complete their trip. $M_{11}(t)$ and $M_{22}(t)$ represent the rate at which travelers complete their trips within the first and second regions, respectfully, and are shown in Equations (20-21). The summation of $M_{11}(t) + M_{22}(t)$ yields the rate at which vehicles complete their trips within the entire urban network. $M_{12}(t)$ and $M_{21}(t)$ are the transfer functions from the first to second region and second to first region in time period t, which represent the rates at which vehicles switch between regions, and are expressed in Equations (22-23).

$$M_{11}(t) = \left(\frac{n_{11}(t) * G_1(n_1(t))}{n_1(t)}\right) \quad (20)$$

$$\mathrm{M}_{22}(\mathrm{t}) = \left(\frac{n_{22}(t) * G_2(n_2(t))}{n_2(t)}\right) \quad (21)$$

$$M_{12}(t) = \frac{n_{12}(t) * G_1(n_1(t))}{n_1(t)} \quad (22)$$

$$M_{21}(t) = \frac{n_{21}(t) * G_2(n_2(t))}{n_2(t)} \quad (23)$$

NUMERICAL EXAMPLE

A case study example is used to illustrate the benefits of VSL and combining VSL with gating, as well as to test the stability of the proposed control with respect to fluctuations in travel demand and the MFD. For the purposes of this study, both regions are assumed to share the same MFD, which is a re-scaled and adjusted version of the MFD for Yokohama, Japan as provided in (*41*). The congested branch is specifically adjusted so it is linear so that the MFD is concave and is equal to zero at the jam accumulation. The functional form of the MFD considered is:

$$G\big(n(t)\big) = \begin{cases} \big((2.052e^{-7} * n^3) - (2.586e^{-3} * n^2) + (9.58 * n)\big), & 0 < n < 4{,}666 \\ \big(15{,}714.233 - (1.38655 * n)\big), & 4{,}667 < n < 11{,}333 \end{cases} \quad (24)$$

From Equation (24) we see that the critical accumulation in each region is $2{,}710\ veh$ and this is associated with a maximum trip completion rate of $3.07\ veh/sec$. The maximum accumulation in each region is $11{,}333\ veh$.

Traffic on the freeway is assumed to obey a fundamental diagram with free flow speed of 60 mi/hr, capacity of 11,000 veh/hr and backward wave speed of -10 mi/hr. A constant time-step of $\Delta t = 1$ minute is assumed with a control horizon of $N_c = 2$ time steps and a prediction horizon of $N_p = 30$ time steps when implementing the MPC framework. A discussion of how the MPC was tuned for this optimization problem is shown below. Furthermore, adopted speed limits are assumed to be held constant for at least 5 minutes to ensure that speed limits do not change too rapidly. Finally, speed limits are assumed to change gradually (e.g., in 10 mi/hr increments) to avoid sudden speed changes, and are restricted to three possible values (specifically 60, 50, and 40 mi/hr). Additional constraints are added to ensure lower and upper bounds of the accumulations within each region, and minimum and maximum control constraints are met. A lower bound of 0.5 for perimeter metering control is implemented to avoid situations in which vehicles are restricted entirely from traveling between urban regions. These constraints are shown below.

0	minimum accumulation in the urban regions
11,333	maximum accumulation in the urban region
0.5	minimum perimeter control constraint
0.9	maximum perimeter control constraint

The optimization problems are solved heuristically using particle swarm optimization. Since its introduction in 1995 (*42*), the PSO algorithm has been adjusted to suit a variety of needs. It has proven to be effective at solving single objective and multi objective, mixed integer nonlinear programs (*43*) and is popular due to its low computational cost and the speed at which it can be implemented. Extensive tests were performed to ensure that the PSO was properly tuned so that optimal solutions were achieved for this problem, a discussion of this process is presented below.

Tuning the MPC and PSO Parameters

Before utilizing the model predictive controller and particle swarm optimization, parameters need to be tuned so we are sure the controller and solver are effective for the optimization problem at hand. As mentioned previously, two parameters dictate how the MPC operates; a control horizon (Nc) and a prediction horizon (Np). In previous literature, the values Nc = 2 and Np = 20 were used optimizing a similar perimeter metering problem (*40*). Because the problem outlined in this paper is different than that in previous work, it is necessary to perform an analysis to tune the parameters used in the MPC. Three different control horizons and a range of prediction horizons were used to solve the same optimization problem. The solution obtained from the lowest prediction horizon was considered as the base solution. Figure 3a provides the relative improvement in operational performance as a function of the prediction horizon. Notice that for each control horizon, the performance improves by increasing the prediction horizon. Moreover, there is a prediction horizon value where the relative solution improvement plateaus. Because a control horizon of 2 consistently yielded higher percent improvement in solution, it was chosen as the control horizon for the MPC used in this analysis. This is likely due to larger control horizons having a larger solution space. The relative improvement in solutions corresponding to the control horizon of 2 plateaus around a prediction horizon of 30 time steps. Following this analysis, values of 2 and 30 are chosen as the control and prediction horizons, respectively.

Similar to the process used to tune the MPC parameters, the number of iterations and population size used in the PSO solver were tuned for the analysis presented in this paper. In addition to the percent relative improvement in solutions, the computation time was also considered for the values of each parameter. This addition is due to the fact that increasing the number of iterations and population size has a large impact on the computation time required to solve the problem. Again, the relative improvement plateaus at a certain value of each parameter, as the computation time continues to increase exponentially. From Figure 3b and 3c, it is observable that at 60 iterations and a population size of 150, the relative improvement begins to plateau. While larger values of each parameter result in a slightly increased relative improvement, the increasing computation time leads us to choose these values in an effort to keep the solution effective considering real time scenarios.

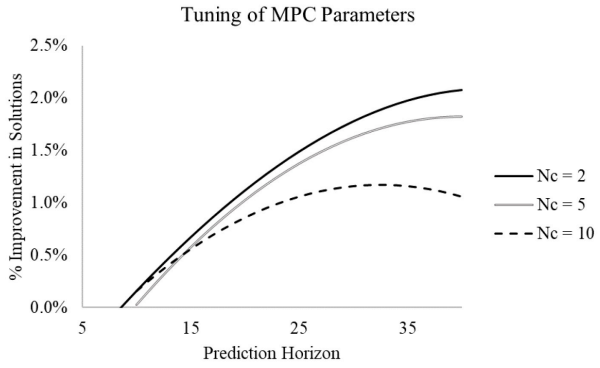

(a) Tuning prediction and control horizons of MPC

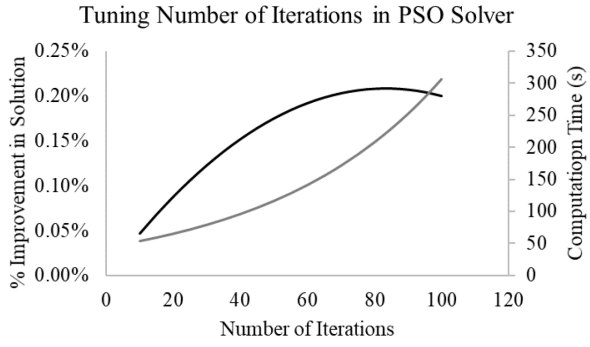

(b) Tuning number of iterations in PSO solver

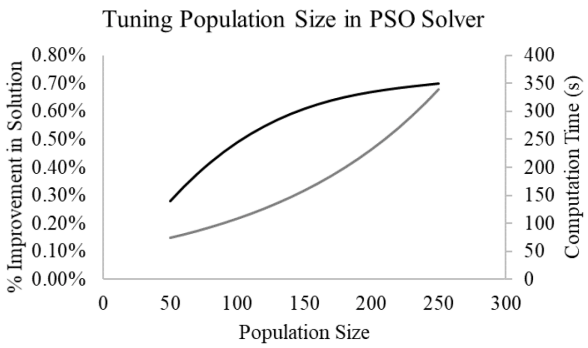

(c) Tuning population size in PSO solver

Figure 3. Graphical understanding of how changing MPC and PSO parameters impacts the solution to the optimization problem

Benefit of VSL Control and Coordinated Control

The numerical example considered here focuses on a case in which VSL alone and the combination of VSL and perimeter metering control provide benefits to traffic in the mixed network. This will occur when the congestion in the urban network is primarily due to the demand exiting the freeway, along with a peak in internal and external demands within each urban region. Due to the multifaceted aspect of the demand in the network as well as the impact of route choice, both VSL and perimeter metering control have the capacity to reduce congestion in the mixed network. Figures 4a and 4b provide the demand profiles adopted for the first and second numerical tests presented in this paper, respectively. All exogeneous and endogenous urban network demands, and freeway demands are assumed to peak over the course of a 20-minute period, mimicking a morning rush. Traffic in the urban regions is described by the same MFD, expressed previously in equation (*24*).

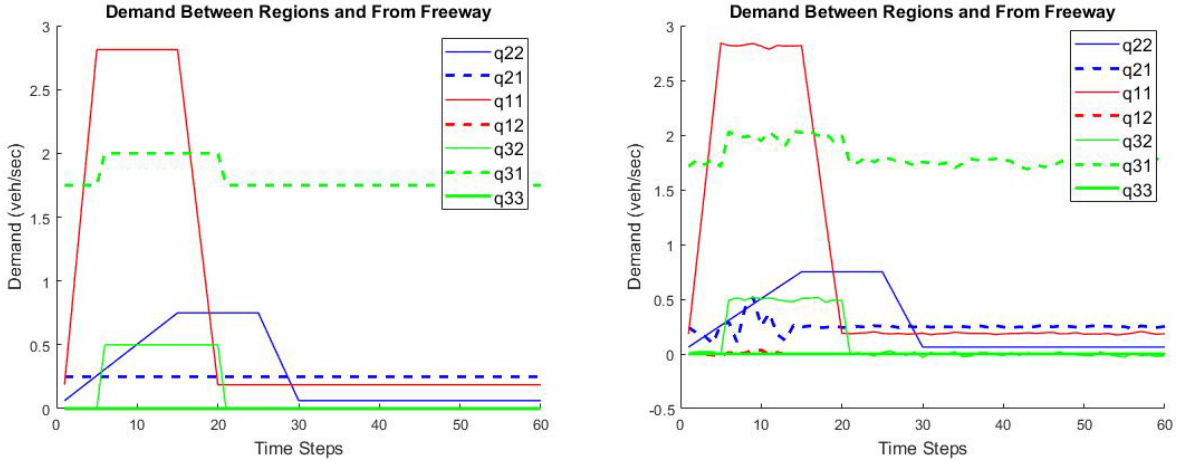

(a) Demand profile used in first numerical simulation

(b) Demand profile used in second numerical simulation

Figure 4. Demands used in first and second numerical simulations

First, we consider the scenario when no control is implemented. In Figure 5a, we can see the accumulation in the second region increases past the critical accumulation and becomes congested due to the incoming traffic from the freeway, the internal demands, and the demands from the second to the first region. Region 1 remains uncongested during the study period. Once the demand within and between the urban regions decreases, the second region slowly becomes uncongested. Without any control implemented, travelers experience 5,450.5 vehicle-hours of total travel time.

Next, consider the case where VSL control is implemented. Due to the large spike in demands that occurs early in the study period, the freeway speed limit (Figure 5e) is lowered at the sixth and eleventh time steps. In Figure 5b, we can see region 2 becomes congested soon after time step 5, when the speed limit is lowered to limit traffic exiting the freeway. At the end of the study period, the speed limit is not increased back up to the free flow speed. This could be because the second region does not become fully uncongested by the end of the study period (as seen in Figure 5b). Compared to the no control scenario, implementing VSL control reduces total travel time by approximately 2.17%, as shown in Figure 5b. The scenario with perimeter metering control outperforms the scenario with VSL alone and provides a reduction in total travel time compared to the no control scenario of approximately 4.12%. Vehicles from region 1 are kept from entering region 2 from time steps 9 to 50. During this nearly 40-minute period, vehicles from the uncongested region 1 are limited from entering the congested region 2, as shown in Figure 5c, which allows region 2 to approach an uncongested state. This control allows the entire network to become much less congested by the end of the study period.

Finally, consider the simultaneous implementation of both VSL and perimeter metering control. Because this case study includes a peak in demand from the freeway into the first region, as well as demands from region 2 to region 1, it is expected that a combination of the two control strategies will be more effective than either strategy on its own. Looking at Figure 5d, this is shown to be the case. Combining the two types of control (shown in Figure 6a and Figure 6b) results in a total travel time of 5,161.8 vehicle-hours, which represents a savings in total travel time of about 5.30% compared to the no control scenario. This is a large reduction compared to the no control

case (over 250 vehicle-hours), and significant reductions compared to VSL alone and perimeter metering alone (over 150 vehicle-hours and over 60 vehicle-hours, respectively). The perimeter metering control implemented in the combined control scenario limits the vehicles allowed to exit region 2 from region 1 for time steps 9 (when region 1 becomes uncongested following the peak in demands) through 40 (when the VSL increases back up to the free flow speed, and the second region is steadily becoming uncongested following the peak in demands). This same analysis can be discussed for the VSL control occurring with the perimeter metering. The only difference between this VSL control and the VSL control implemented on its own discussed previously, is that the speed limit is stepped back up to the original speed limit at the end of the study period. This is likely due to the added benefit provided by the perimeter metering control.

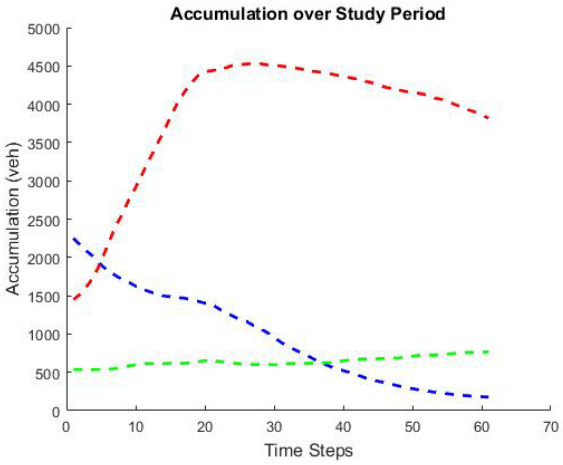

(a) No Control
(TTT = 5,450.5 veh-hrs)

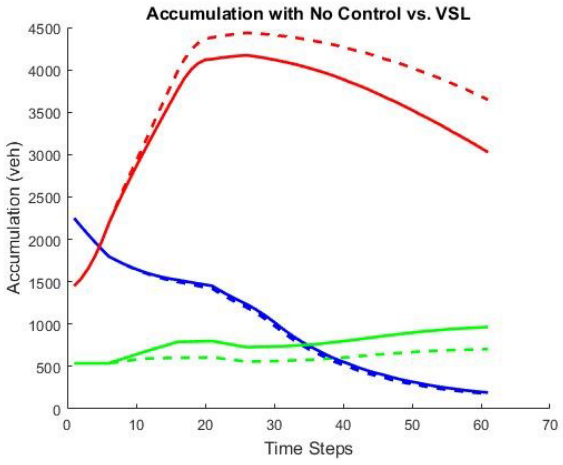

(b) VSL Control Only
(TTT = 5332 veh-hrs)

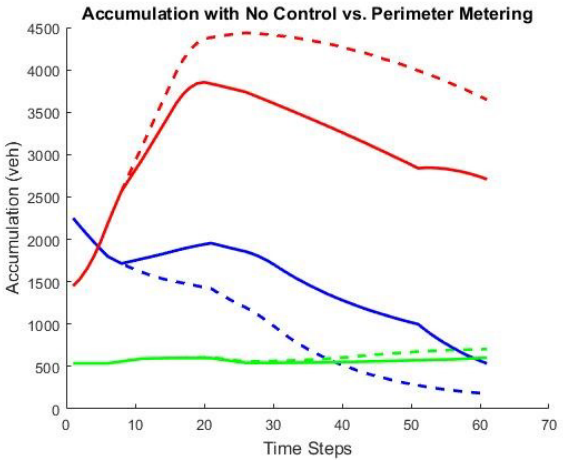

(c) Perimeter Metering Control Only
(TTT = 5,225.9 veh-hrs)

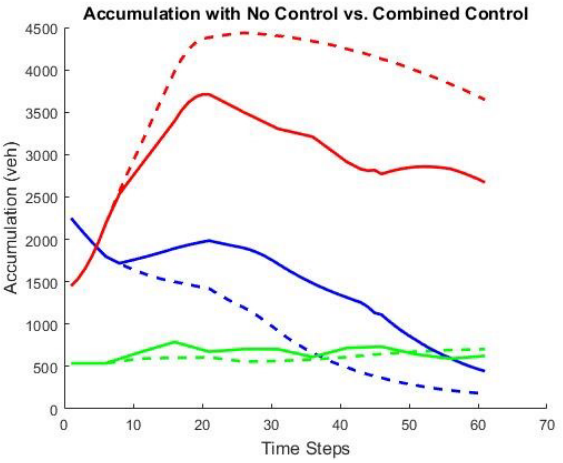

(d) VSL and Perimeter Metering
(TTT = 5,161.8 veh-hrs)

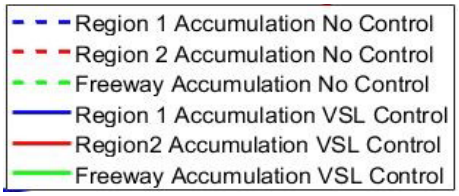

Figure 5. Accumulation and total travel time for four different control scenarios

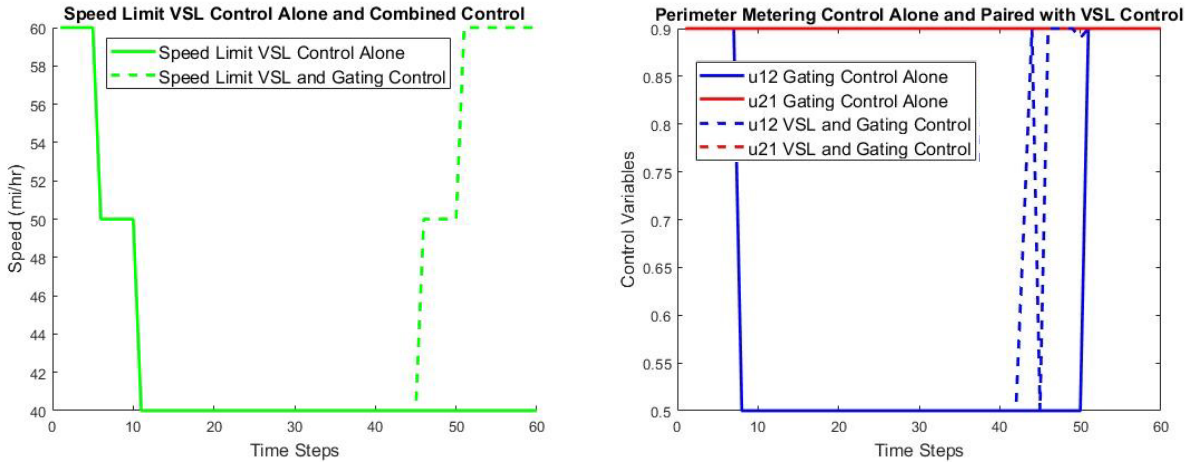

(a) VSL control implemented alone and with perimeter metering control

(b) Perimeter metering control implemented alone and with VSL control

Figure 6. Control actions implemented during three different control scenarios in first numerical example

Stability of Control to Fluctuations in Demand and MFD Errors

The numerical example proves to show that implementation of variable speed limit on its own is effective in managing congestion caused by exiting freeway traffic and that the coordination of VSL and perimeter metering control is even more effective to the same end than implementation of either control on their own. An extension of the example is shown below to examine the stability of these control strategies when errors are present in the demands and in the MFD that are applied within the optimization framework. To incorporate error into the demands, we assume that the actual demand is equal to the estimated demand that is input into the algorithm plus a normally distributed error term with mean zero and standard deviation equal to five percent of the estimated demand at each time step. The same type of error is added to the MFD, where the standard deviation of the error term is equal to five percent of the average trip completion rate at each time step. This is more realistic than the previous example because while we can estimate the average traffic demands and trip completion rates, in real life these values fluctuate randomly. In this more realistic example, the MPC considers average demands and trip completion rates as presented in the previous example, while the real-life simulation operates with errors present in the demand and the MFD. In order to gain a solid understanding of how these control scenarios run considering stochastic demands and MFDs, this example was repeated twenty separate times to determine if the proposed control can still provide travel time savings in a stochastic environment. A sample

run of this example for the demands in Scenario 1 is summarized in Figure 4b, Figure 7, and Figure 8.

Again, we compare the total travel times of four different control scenarios: no control, VSL only, perimeter metering only, and both VSL and perimeter metering control. A sample of the accumulation and total travel time for the four scenarios is shown in Figure 8, and the control actions implemented for the different scenarios are shown in Figure 9.

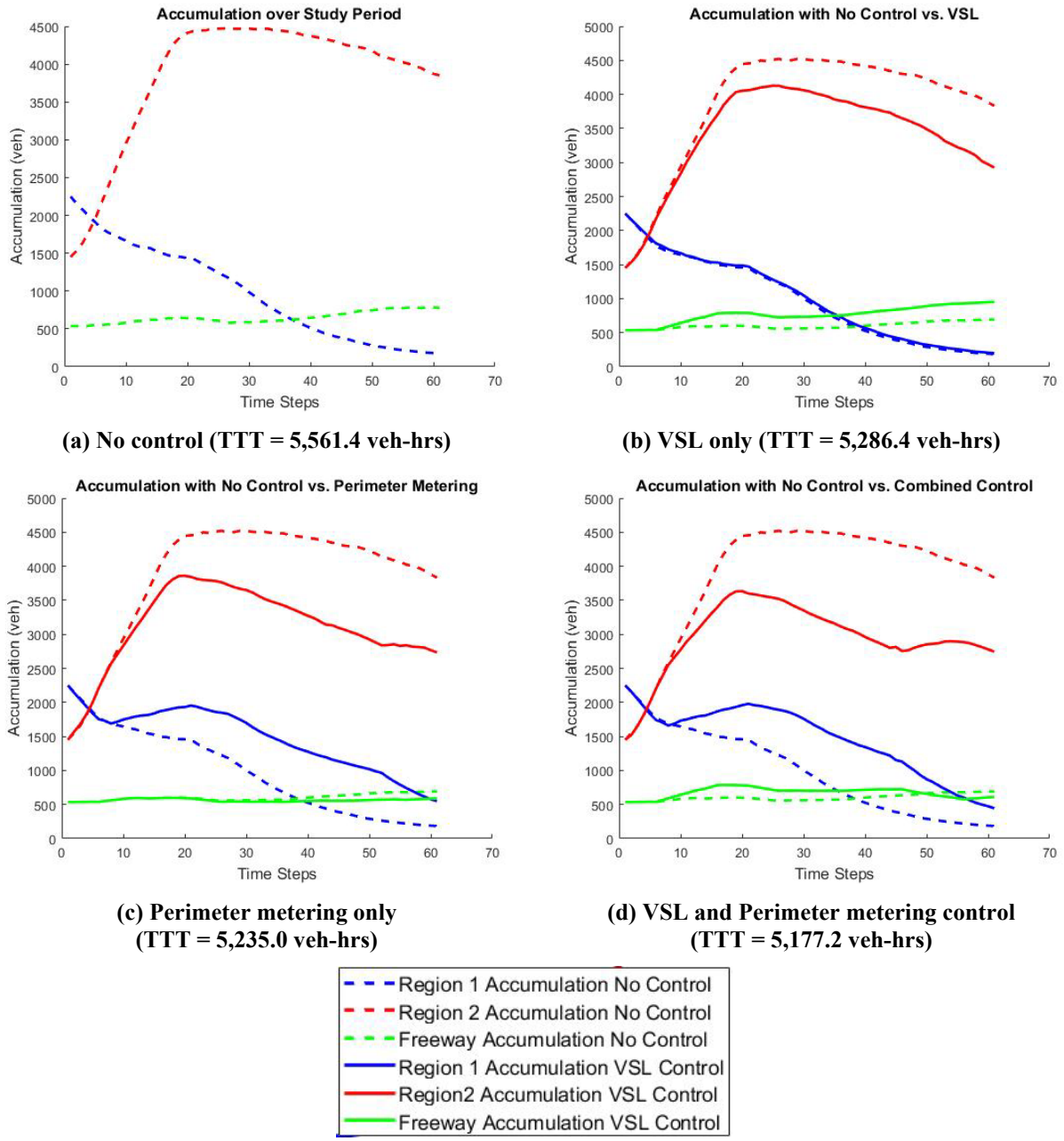

(a) No control (TTT = 5,561.4 veh-hrs)

(b) VSL only (TTT = 5,286.4 veh-hrs)

(c) Perimeter metering only (TTT = 5,235.0 veh-hrs)

(d) VSL and Perimeter metering control (TTT = 5,177.2 veh-hrs)

Figure 7. Accumulation and total travel time under different control scenarios

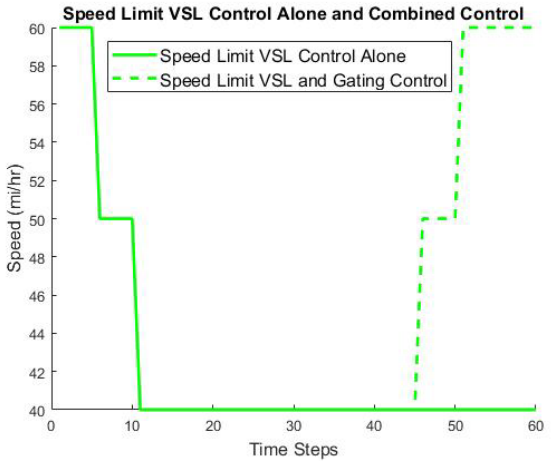

(e) **VSL control implemented alone and with perimeter metering control**

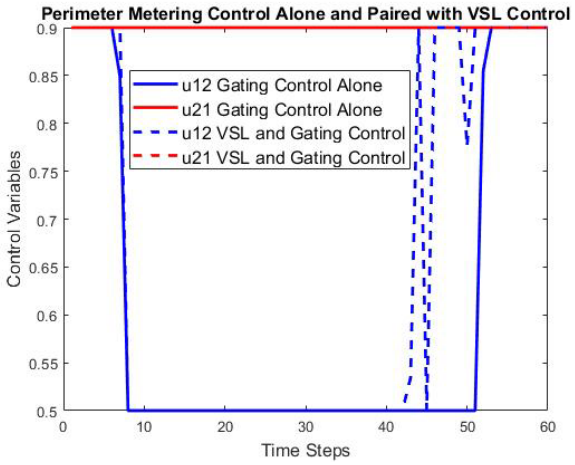

(f) **Perimeter metering control implemented alone and with VSL control**

Figure 8. Control actions implemented during three different control scenarios in second numerical example

The average total travel times and standard errors for each control scheme are presented below.

No Control:	Mean TTT = 5,462.04 veh-hr	Standard Error = 12.67
VSL Control:	Mean TTT = 5,336.71 veh-hr	Standard Error = 18.78
No Control vs VSL:	Change in TTT = 125.33 veh-hr	% Reduction = 2.29%
Perimeter Metering Control:	Mean TTT = 5,233.25 veh-hr	Standard Error = 12.43
No Control vs Perimeter Metering:	Change in TTT = 228.79 veh-hr	% Reduction = 4.19%
Combined Control:	Mean TTT = 5,155.325veh-hr	Standard Error = 14.97
No Control vs Combined:	Change in TTT = 306.71 veh-hr	% Reduction = 5.62%

Adding realistic error terms in the demand and the MFD results in different total travel times for all four control scenarios compared to the previous example. The same trends observed in the second numerical example are seen here; implementing VSL control lowers the total travel time compared to the no control scenario, perimeter metering control on its own is more beneficial than VSL control alone, and the combination of VSL and perimeter metering control is more effective at managing congestion than either control strategy alone. All differences are statistically significant and thus not simple due to random fluctuations in demand.

DISCUSSION AND FUTURE WORK

This paper presents a framework for congestion management in a mixed freeway-urban network that applies both perimeter metering control and variable speed limits (VSL). The variable speed

limits are used to limit vehicle flow from the freeway to the urban network, which allows vehicles to queue on a freeway instead of on the surface streets where their presence might reduce overall network productivity. The impact of variable speed limits on freeway traffic dynamics are described using kinematic wave theory, which provides the minimum speed limits and length of the freeway over which the variable speed limits must be applied. Reductions in speed limit are found to temporarily reduce the rate vehicles can exit the freeway and enter the urban network, while increases in speed limit do the opposite. These changes in flow can be described mathematically, which allows the impacts of VSL to be integrated into an optimization problem to reduce total travel time within the combined network. The joint perimeter control and variable speed limit optimization problem can then be solved using a model predictive control framework. Several numerical tests are performed that demonstrate the scenarios under which 1) VSL would effectively improve network conditions and 2) VSL and perimeter control could complement each other to further improve network operations.

Future work will consider internal signal control mechanisms within each region of the urban network. For example, previous work (*30*) has shown the MFD of an urban network changes drastically when left turns are prohibited, making strategic left turn prohibition another possible congestion management strategy to implement alongside VSL and perimeter metering control. A joint strategy that combines three options could provide even superior benefits to the combined mixed freeway-urban network.

ACKNOWLEDGEMENTS

This research was supported by NSF Grant CMMI-1749200.

AUTHOR CONTRIBUTIONS

The authors confirm contribution to the paper as follows: study conception and design: RY, VG; analysis and interpretation of results: RY, VG; draft manuscript preparation: RY, VG. All authors reviewed the results and approved the final version of the manuscript.

REFERENCES

1. Hegyi, A., B. De Schutter, and H. Hellendoorn. Model Predictive Control for Optimal Coordination of Ramp Metering and Variable Speed Limits. *Transportation Research Part C: Emerging Technologies*, Vol. 13, No. 3, 2005, pp. 185–209. https://doi.org/10.1016/J.TRC.2004.08.001.

2. Bellemans, T., B. De Schutter, and B. De Moor. Model Predictive Control for Ramp Metering of Motorway Traffic: A Case Study. *Control Engineering Practice*, Vol. 14, No. 7, 2006, pp. 757–767. https://doi.org/10.1016/J.CONENGPRAC.2005.03.010.

3. Gayah, V. V., C. D. Santos, M. Abdel-Aty, A. Dhindsa, and J. Dilmore. Evaluating ITS Strategies for Real-Time Freeway Safety Improvement. *IEEE Conference on Intelligent Transportation Systems, Proceedings, ITSC*, 2006.

4. Abdel-Aty, M., R. J. Cunningham, V. V. Gayah, and L. Hsia. Dynamic Variable Speed Limit Strategies for Real-Time Crash Risk Reduction on Freeways. *Transportation Research Record*, No. 2078, 2008. https://doi.org/10.3141/2078-15.

5. Chen, D., and S. Ahn. Variable Speed Limit Control for Severe Non-Recurrent Freeway Bottlenecks. *Transportation Research Part C: Emerging Technologies*, Vol. 51, 2015, pp. 210–230. https://doi.org/10.1016/J.TRC.2014.10.015.

6. Han, Y., D. Chen, and S. Ahn. Variable Speed Limit Control at Fixed Freeway Bottlenecks Using Connected Vehicles. *Transportation Research Part B: Methodological*, Vol. 98, 2017, pp. 113–134. https://doi.org/10.1016/J.TRB.2016.12.013.

7. Papageorgiou, M., C. Diakaki, V. Dinopoulou, A. Kotsialos, and Y. Wang. Review of Road Traffic Control Strategies. No. 91, 2003, pp. 2043–2065.

8. Robertson, D. I., and R. D. Bretherton. Optimizing Networks of Traffic Signals in Real Time—The SCOOT Method. *IEEE Transactions on Vehicular Technology*, Vol. 40, No. 1, 1991, pp. 11–15. https://doi.org/10.1109/25.69966.

9. Xie, X. F., S. F. Smith, L. Lu, and G. J. Barlow. Schedule-Driven Intersection Control. *Transportation Research Part C: Emerging Technologies*, Vol. 24, 2012, pp. 168–189. https://doi.org/10.1016/j.trc.2012.03.004.

10. Mirchandani, P., and L. Head. A Real-Time Traffic Signal Control System: Architecture, Algorithms, and Analysis. *Transportation Research Part C: Emerging Technologies*, 2001. https://doi.org/10.1016/S0968-090X(00)00047-4.

11. Godfrey, J. W. The Mechanism of a Road Network. *Traffic Engineering & Control*, Vol. 11, No. 7, 1969, pp. 323–327.

12. Mahmassani, H., J. C. Williams, and R. Herman. Investigation of Network-Level Traffic Flow Relationships: Some Simulation Results. *Transportation Research Record: Journal of the Transportation Research Board*, Vol. 971, 1984, pp. 121–130.

13. Geroliminis, N., and C. F. Daganzo. Existence of Urban-Scale Macroscopic Fundamental Diagrams: Some Experimental Findings. *Transportation Research Part B: Methodological*, Vol. 42, No. 9, 2008, pp. 759–770.

14. Geroliminis, N., and J. Sun. Properties of a Well-Defined Macroscopic Fundamental Diagram for Urban Systems. *Transportation Research Part B*, Vol. 45, No. 3, 2011, pp. 605–617. https://doi.org/10.1016/j.trb.2010.11.004.

15. Daganzo, C. F., V. V. Gayah, and E. J. Gonzales. Macroscopic Relations of Urban Traffic Variables: Bifurcations, Multivaluedness and Instability. *Transportation Research Part B: Methodological*, Vol. 45, No. 1, 2011, pp. 278–288.

16. Daganzo, C. F. Urban Gridlock: Macroscopic Modeling and Mitigation Approaches. *Transportation Research Part B: Methodological*, Vol. 41, No. 1, 2007, pp. 49–62.

17. Haddad, J., and N. Geroliminis. On the Stability of Traffic Perimeter Control in Two-Region Urban Cities. *Transportation Research Part B: Methodological*, Vol. 46, No. 9, 2012, pp. 1159–1176.

18. Keyvan-Ekbatani, M., A. Kouvelas, I. Papamichail, and M. Papageorgiou. Exploiting the Fundamental Diagram of Urban Networks for Feedback-Based Gating. *Transportation Research Part B: Methodological*, Vol. 46, No. 10, 2012, pp. 1393–1403.

19. Aboudolas, K., and N. Geroliminis. Perimeter and Boundary Flow Control in Multi-

Reservoir Heterogeneous Networks. *Transportation Research Part B: Methodological*, Vol. 55, 2013, pp. 265–281.

20. Haddad, J., and Z. Zheng. Adaptive Perimeter Control for Multi-Region Accumulation-Based Models with State Delays. *Transportation Research Part B: Methodological*, 2018. https://doi.org/10.1016/j.trb.2018.05.019.

21. Yang, K., M. Menendez, and N. Zheng. Heterogeneity Aware Urban Traffic Control in a Connected Vehicle Environment: A Joint Framework for Congestion Pricing and Perimeter Control. *Transportation Research Part C: Emerging Technologies*, Vol. 105, 2019, pp. 439–455. https://doi.org/10.1016/j.trc.2019.06.007.

22. Haitao, H., K. Yang, H. Liang, M. Menendez, and S. I. Guler. Providing Public Transport Priority in the Perimeter of Urban Networks: A Bimodal Strategy. *Transportation Research Part C: Emerging Technologies*, Vol. 107, 2019, pp. 171–192. https://doi.org/10.1016/j.trc.2019.08.004.

23. Zhou, D., and V. V. Gayah. Model-Free Perimeter Metering Control for Two-Region Urban Networks Using Deep Reinforcement Learning. *Transportation Research Part C: Emerging Technologies*, Vol. 124, 2021, p. 102949. https://doi.org/10.1016/j.trc.2020.102949.

24. Geroliminis, N., and D. M. Levinson. Cordon Pricing Consistent with the Physics of Overcrowding. In *18th International Symposium on Transportation and Traffic Theory*, Springer.

25. Gonzales, E. J., and C. F. Daganzo. Morning Commute with Competing Modes and Distributed Demand: User Equilibrium, System Optimum, and Pricing. *Transportation Research Part B: Methodological*, Vol. 46, No. 10, 2012, pp. 1519–1534.

26. Simoni, M. D., A. J. Pel, R. A. Waraich, and S. P. Hoogendoorn. Marginal Cost Congestion Pricing Based on the Network Fundamental Diagram. *Transportation Research Part C: Emerging Technologies*, Vol. 56, 2015, pp. 221–238.

27. Zheng, N., R. A. Waraich, K. W. Axhausen, and N. Geroliminis. A Dynamic Cordon Pricing Scheme Combining the Macroscopic Fundamental Diagram and an Agent-Based Traffic Model. *Transportation Research Part A: Policy and Practice*, Vol. 46, No. 8, 2012, pp. 1291–1303.

28. Gayah, V. V., and C. F. Daganzo. Analytical Capacity Comparison of One-Way and Two-Way Signalized Street Networks. *Transportation Research Record: Journal of the Transportation Research Board*, No. 2301, 2012, pp. 76–85.

29. Ortigosa, J., V. V. Gayah, and M. Menendez. Analysis of One-Way and Two-Way Street Configurations on Urban Grids. *Transportmetrica B: Transport Dynamics*, Vol. 7, No. 1, 2019, pp. 61–81.

30. Ortigosa, J., V. V. Gayah, and M. Menendez. Analysis of Network Exit Functions for Various Urban Grid Network Configurations. *Transportation Research Record: Journal of the Transportation Research Board*, No. 2491, 2015, pp. 12–21.

31. DePrator, A., O. Hitchcock, and V. V. Gayah. Improving Urban Street Network Efficiency by Prohibiting Left Turns at Signalized Intersections. *Transportation Research Record:*

Journal of the Transportation Research Board, Vol. 2622, No. 1, 2017, pp. 58–69.

32. Knoop, V. L., S. P. Hoogendoorn, and J. W. C. Van Lint. Routing Strategies Based on Macroscopic Fundamental Diagram. *Transportation Research Record: Journal of the Transportation Research Board*, Vol. 2315, No. 1, 2012, pp. 1–10.

33. Yildirimoglu, M., and N. Geroliminis. Approximating Dynamic Equilibrium Conditions with Macroscopic Fundamental Diagrams. *Transportation Research Part B: Methodological*, Vol. 70, 2014, pp. 186–200.

34. Haddad, J., M. Ramezani, and N. Geroliminis. Cooperative Traffic Control of a Mixed Network with Two Urban Regions and a Freeway. *Transportation Research Part B: Methodological*, Vol. 54, 2013, pp. 17–36.

35. Ji, Y., and N. Geroliminis. On the Spatial Partitioning of Urban Transportation Networks. *Transportation Research Part B: Methodological*, Vol. 46, No. 10, 2012, pp. 1639–1656.

36. Cho, H., and Y. Kim. Analysis of Traffic Flow with Variable Speed Limit on Highways. *KSCE Journal of Civil Engineering*, Vol. 16, No. 6, 2012, pp. 1048–1056. https://doi.org/10.1007/s12205-012-1395-x.

37. Lighthill, M. J., and G. B. Whitham. On Kinematic Waves. I. Flood Movement in Long Rivers. *Proceedings of the Royal Society of London. Series A. Mathematical and Physical Sciences*, Vol. 229, No. 1178, 1955, pp. 281–316.

38. Lighthill, M. J., and G. B. Whitham. On Kinematic Waves. II. A Theory of Traffic Flow on Long Crowded Roads. *Proceedings of the Royal Society of London. Series A. Mathematical and Physical Sciences*, Vol. 229, No. 1178, 1955, pp. 317–345.

39. Richards, P. I. Shock Waves on the Highway. *Operations Research*, Vol. 4, No. 1, 1956, pp. 42–51.

40. Gayah, V. V., E. T. Donnell, Z. Yu, and L. Li. Safety and Operational Impacts of Setting Speed Limits below Engineering Recommendations. *Accident Analysis and Prevention*, Vol. 121, 2018, pp. 43–52. https://doi.org/10.1016/j.aap.2018.08.029.

41. Geroliminis, N., J. Haddad, M. Ramezani, and N. Geroliminis. Optimal Perimeter Control for Two Urban Regions with Macroscopic Fundamental Diagrams: A Model Predictive Approach. *Intelligent Transportation Systems, IEEE Transactions on*, Vol. 14, No. 1, 2013, pp. 348–359.

42. Kennedy, J., and R. Eberhart. Particle Swarm Optimization. No. 4, pp. 1942–1948.

43. Shokrian, M., and K. A. High. Application of a Multi Objective Multi-Leader Particle Swarm Optimization Algorithm on NLP and MINLP Problems. *Computers and Chemical Engineering*, Vol. 60, 2014, pp. 57–75. https://doi.org/10.1016/j.compchemeng.2013.08.004.